Focusing of an aberrated radially polarized beam by microscope objectives

Rafael G. González-Acuña[a,*] **and Simon Thibault**[a,b]
aIndependent Researcher, Santa Catarina, México
bUniversité Laval, Centre d'optique, photonique et laser, Quebec City, Canada

ABSTRACT. A rigorous method is presented to compute the vector diffraction pattern of microscope objectives considering on-axis aberrated and radially polarized wavefronts. For that, the diffraction pattern of the microscope objective is computed considering the polarization and the wavefront at the exit pupil of the optical system. These computations do not assume that at the exit pupil of the microscope objective the wavefront is spherical but aberrated. Examples of real microscope objectives' performance are presented.

1 Introduction

The first theories that described diffraction did not consider the vectorial nature of the electric field and magnetic field.[1] These theories are the Rayleigh–Sommerfeld and scalar Kirchhoff models.[2] Despite considering the electric field as a scalar quantity, these theories were available to describe the beam propagation on paraxial optical systems. A particular case of the scalar Kirchhoff model is the Fraunhofer approximation for far fields.[1,2] The Fraunhofer approximation can compute the diffraction pattern of optical systems, the point-spread function, and the Airy disc.[3] The Airy disc described the best-focused spot of light that a perfect optical system with a circular aperture could make, given that it is diffraction-limited.[1,2]

The Airy disc described by the Fraunhofer approximation is not the smallest possible spot. The spot size can be decreased if the vectorial nature of light is considered. Richards and Wolf obtained diffraction integral to describe the beam propagation considering the polarization of light.[4,5] Using the Richards–Wolf integral with radially polarized light the Airy disc can be decreased. Therefore, the Richards–Wolf integral is used to describe the diffraction pattern beyond the limits imposed by the scalar theories. This treatment, beyond the scalar approximation, is necessary in several areas of science, including high-resolution microscopy,[6–9] optical trapping,[10] electron acceleration,[11] optical vortex knots,[12,13] beam shaping, etc.[14–21]

Nevertheless, the Richards–Wolf integral only considers perfect spherical wavefronts[4,5] and real optical systems do not generate perfect spherical wavefronts at the exit pupil, but aberrated wavefronts. A new diffraction integral has been published in Refs. 22 and 23 and this integral can compute the diffraction pattern of vectorial aberrated wavefronts with radial polarization. Here, the model presented in Ref. 23 is used to compute the diffraction pattern of several microscope objectives considering the polarization of the wavefront and its aberrations. The work in Ref. 23 differs from the models presented in Refs. 15, 24, and 25 that the aberrations are taken directly

---

*Address all correspondence to Rafael G. González-Acuña, rafael.guillermo.ga@gmail.com

from the wavefront using the Malus–Dupin theorem,[23] instead of considering the aberration function as an additional phase in over a spherical wavefront.[15,24,25] This manuscript aims to present a rigorous method to compute the vector diffraction pattern of microscope objectives considering on-axis aberrated and radially polarized wavefronts.

2 Vectorial Diffraction Integral

Ref. 23 presents a new vector diffraction integral capable of computing the diffraction patterns for aspheric and freeform wavefronts, with any polarization. This paper does not consider an arbitrary polarization state since working with arbitrary polarization states is not straightforward, and it highly increases the complexity of the problem. The deduction of these integral starts from the angular spectrum representation of the optical fields. Like the Richards-Wolf integral, the integral presented in Ref. 23 is formulated by the assumption that the diffraction pattern is computed by the superposition of plane waves, and the contribution of evanescent waves is ignored. This integral is given as

$$
\begin{aligned}
\mathbf{E}(r,\phi,z) = & \frac{E_0 k}{2\pi} \int_{y_{\min}}^{y_{\max}} \int_{x_{\min}}^{x_{\max}} P(x,y)q(x,y)l_0(x,y) \left[\frac{\partial_x^2 w \partial_y^2 w - (\partial_{xy}w)^2}{(\partial_x w^2 + \partial_y w^2 + 1)^{3/2}} \right] \\
& \times \left[\frac{\frac{\cos\theta\partial_x w}{\sqrt{\partial_x w^2 + \partial_y w^2 + 1}} - \sin\theta\partial_y w}{\sqrt{\partial_x w^2 + \partial_y w^2}} \hat{\mathbf{x}} + \frac{\frac{\cos\theta\partial_y w}{\sqrt{\partial_x w^2 + \partial_y w^2 + 1}} + \sin\theta\partial_x w}{\sqrt{\partial_x w^2 + \partial_y w^2}} \hat{\mathbf{y}} \right. \\
& \left. + \cos\theta \sqrt{1 - \frac{1}{\partial_x w^2 + \partial_y w^2 + 1}} \hat{\mathbf{z}} \right] \\
& \times \exp\left[\frac{-izk}{\sqrt{\partial_x w^2 + \partial_y w^2 + 1}} - \frac{ir\cos\phi k\partial_y w}{\sqrt{\partial_x w^2 + \partial_x w^2 + 1}} - \frac{ir\sin\phi k\partial_y w}{\sqrt{\partial_x w^2 + \partial_y w^2 + 1}} \right] \mathrm{d}x\mathrm{d}y, \quad (1)
\end{aligned}
$$

where $\mathbf{E}(r,\phi,z)$ is the electric field in cylindrical coordinates (r,ϕ,z), and $\hat{\mathbf{x}}$, $\hat{\mathbf{y}}$, and $\hat{\mathbf{z}}$, are the unit vectors in the x, y, and z directions. E_0 is a constant amplitude, $q(x,y)$ is the apodization function, k is the wave number. The wavefront $w(x,y)$ must be a continuous function of how independent variables are x and y. l_0 is the illumination function. $\partial_x w$ and $\partial_y w$ are the partial derivatives of $w(x,y)$ respect to are x and y. $P(x,y)$ is the exit pupil shape, a function that inside the pupil region is 1 and 0 otherwise. This region is delimited by $x_{\min}$ and $x_{\max}$ and $y_{\min}$ and $y_{\max}$ in the x and y directions, respectively. θ is the rotation angle along the plane perpendicular to $\mathbf{k}$. Depending on the value of θ is the polarization state, if $\theta = 0$, we get a for a radially symmetric beam

$$
\begin{aligned}
\mathbf{E}(r,\phi,z) = & \frac{E_0}{2\pi} \int_{y_{\min}}^{y_{\max}} \int_{x_{\min}}^{x_{\max}} P(x,y)q(x,y)l_0(x,y) \left[\frac{\partial_x^2 w \partial_y^2 w - (\partial_{xy}w)^2}{(\partial_x w^2 + \partial_y w^2 + 1)^{3/2}} \right] \\
& \times \left[\frac{\partial_x w \hat{\mathbf{x}} + \partial_y w \hat{\mathbf{y}}}{\sqrt{\partial_x w^2 + \partial_y w^2 + 1}\sqrt{\partial_x w^2 + \partial_y w^2}} + \sqrt{1 - \frac{1}{\partial_x w^2 + \partial_y w^2 + 1}} \hat{\mathbf{z}} \right] \\
& \times \exp\left[\frac{-izk}{\sqrt{\partial_x w^2 + \partial_y w^2 + 1}} - \frac{ir\cos\phi k\partial_x w}{\sqrt{\partial_x w^2 + \partial_x w^2 + 1}} - \frac{ir\sin\phi k\partial_y w}{\sqrt{\partial_x w^2 + \partial_y w^2 + 1}} \right] \mathrm{d}x\mathrm{d}y. \quad (2)
\end{aligned}
$$

In this manuscript, we are going to consider only an input on-axis field, thus the wavefront at the exit pupil is a spherical wavefront with some aberration. Without losing generality these aberrations can be expressed in terms of the Zernike polynomials, and since the field is on-axis and the system is radially symmetric the aberration is aspheric and can be expressed in Zernike terms which are radially symmetric,[26] for example

$$Z_1 = z_1, Z_4 = z_4\sqrt{3}(2\rho^2 - 1), Z_{11} = z_{11}\sqrt{5}(6\rho^4 - 6\rho^2 + 1)$$
$$Z_{22} = z_{22}\sqrt{7}(20\rho^6 - 30\rho^4 + 12\rho^2 - 1), \tag{3}$$

where $\rho^2 = x^2 + y^2$, $x = \rho\cos(\beta)$, and $y = \rho\sin(\beta)$. Z_1, Z_4, Z_{11} and Z_{22} are the 1st, 4th, 11$^{\text{th}}$, and 22nd Zernike terms, and z_1, z_4, z_{11}, and z_{22} their respect coefficients. The method can be generalized to consider more terms. Then, the wavefront at the exit pupil is given as

$$\begin{aligned}
W_{\text{spherical}} - W_{\text{zernike}} = &-\sqrt{R_a^2 - x^2 - y^2} + R_a + \sqrt{5}z_{11}[6([x-1]x + y^2)(x^2 + x + y^2) - 6y^2 + 1] \\
&+ (2x^2 + 2y^2 - 1)[\sqrt{7}z_{22}\{10([x-1]x + y^2)(x^2 + x + y^2) \\
&- 10y^2 + 1\} + \sqrt{3}z_4] + z_1,
\end{aligned} \tag{4}$$

where R_a is the radius of the reference sphere, $W_{\text{spherical}}$ is the reference sphere wavefront, and W_{zernike} is the aberrated wavefront. The result of derivating Eq. (4) respect to x and y is in Eq. (5)

$$\partial_x w = \cos(\beta)\Xi(\rho) \quad \partial_y w = \sin(\beta)\Xi(\rho), \tag{5}$$

where

$$\Xi(\rho) = \frac{1}{\sqrt{R_a^2 - \rho^2}} + 12\sqrt{5}z_{11}(2\rho^2 - 1) + 120\sqrt{7}z_{22}(\rho^2 - 1)\rho^2 + 24\sqrt{7}z_{22} + 4\sqrt{3}z_4. \tag{6}$$

Notice that the partial derivative of $w(x, y)$ for the on-axis field can always be expressed in the form of Eq. (5). There will be always a function $\Xi(\rho)$ that only depends on ρ due to the symmetry. The form of $\Xi(\rho)$ only depends on the number of terms of the Zernike polynomials implemented. If Z_1, Z_4, Z_{11}, and Z_{22} are the only terms considered, lastly the form of $\Xi(\rho)$ is given by Eq. (6).

If the input on-axis field is flat and radially polarized and replacing Eq. (5) in Eq. (2), we get

$$\begin{aligned}
\mathbf{E}(r, \phi, z) = &\frac{E_0}{2\pi}\int_0^{2\pi}\int_0^{\rho_{\max}}\left[\frac{\Xi(\rho)\Xi'(\rho)}{(\Xi(\rho)^2 + 1)^{3/2}}\right]\left[\frac{[\cos(\beta)\hat{\mathbf{x}} + \sin(\beta)\hat{\mathbf{y}}]}{\sqrt{\Xi(\rho)^2 + 1}} + \sqrt{1 - \frac{1}{\Xi(\rho)^2 + 1}}\hat{\mathbf{z}}\right] \\
&\times \exp\left[\frac{-izk}{\sqrt{\Xi(\rho)^2 + 1}} - \frac{ir\cos(\phi)k\cos(\beta)\Xi(\rho)}{\sqrt{\Xi(\rho)^2 + 1}} - \frac{ir\sin(\phi)k\sin(\beta)\Xi(\rho)}{\sqrt{\Xi(\rho)^2 + 1}}\right]q(\rho)l_0(\rho)\mathrm{d}\rho\mathrm{d}\beta,
\end{aligned} \tag{7}$$

where $\Xi'(\rho)$ is the derivative of $\Xi(\rho)$ respect to ρ. Observe that the pupil function has been removed in Eq. (7) and the upper limit of the integral of ρ is one, these results come since the Zernike polynomials are defined in a circle of unity radius. The integral of β in Eq. (7) can be computed using well-known properties of Bessel functions[27]

$$\begin{aligned}
\mathbf{E}(r, z) = &E_0\int_0^{\rho_{\max}}q(\rho)l_0(\rho)\left[\frac{\Xi(\rho)\Xi'(\rho)}{(\Xi(\rho)^2 + 1)^{3/2}}\right]\exp\left[\frac{-izk}{\sqrt{\Xi(\rho)^2 + 1}}\right] \\
&\times \left[\frac{i}{\sqrt{\Xi(\rho)^2 + 1}}J_1\left(\frac{kr\Xi(\rho)}{\sqrt{\Xi(\rho)^2 + 1}}\right)\hat{\mathbf{r}} + \sqrt{1 - \frac{1}{\Xi(\rho)^2 + 1}}J_0\left(\frac{kr\Xi(\rho)}{\sqrt{\Xi(\rho)^2 + 1}}\right)\hat{\mathbf{z}}\right]\mathrm{d}\rho,
\end{aligned} \tag{8}$$

where J_0 and J_1 are the Bessel functions of the zeroth and first-order, respectively. Eq. (8) is the most important equation in the manuscript and it describes the diffraction pattern produced by an aspherical wavefront radially polarized at the exit pupil of an optical system. This integral is expressed in terms of $\Xi(\rho)$, which is the common factor of the partial derivatives of the wavefront at the exit pupil. In this next section, we are going to use Eq. (8) to directly compute the diffraction pattern generated by microscope objectives and test their performance. Equation (8) is more compact and simple than Eq. (2), since it only depends in a single independent parameter. Computationally speaking this is a great advantage over Eq. (2).[23]

3 Illustrative Examples of Diffraction Patterns in Microscopes Objectives

In this section are presented several illustrative examples of diffraction patterns in microscope objectives computed directly using Eq. (8). To use Eq. (8), it is needed to know the shape of the wavefront at the exit pupil of each microscope objective. Since the wavefront at the exit pupil can be expressed in Zernike polynomials, we express the wavefront at the exit pupil with Eq. (4). The coefficients of the Zernike polynomials of a field at the exit pupil of an optical system are computed with commercial optical software. The package used for the examples in this paper is Quadoa Optical CAD.[28] In the following examples, we have set the apodization function q, and the illumination l_0 to be one and the wavelength to be 550 nm.

The first example is a microscope objective that is diffraction-limited according to ray-tracing and the scalar wave theory. This means, all the rays strike from a ray grid inside the Airy disc. Then, the exit pupil is almost a perfect spherical wavefront at the exit pupil, z_1, z_4, z_{11}, z_{22} are close to zero. The coefficients are $z_1 = -2.1815 \times 10^{-08}$ mm, $z_4 = -2.8906 \times 10^{-08}$ mm, $z_{11} = -6.9022 \times 10^{-09}$ mm, and $z_{22} = -5.4309 \times 10^{-09}$ mm. The numerical aperture of the microscope is NA = 0.749. The diffraction pattern in the z-axis and the r are plotted in Fig. 1. The lines that correspond to this example are in dashed orange. The black lines correspond to the classical formulation of Richards–Wolf.[4,5] Observe that for the z-axis and in the r are plotted the orange and black lines overlap on every point. The result then is as predicted by Richards–Wolf.[4,5] It is important to remark that the Richards–Wolf integral is only valid for stigmatic systems. Since the root mean square is much smaller than the Airy disc, the orange line almost overlaps the stigmatic case, the black line. The ray-tracing and stop diagrams are presented in Fig. 2. The grey circle surrounding the stop diagram is the Airy disc
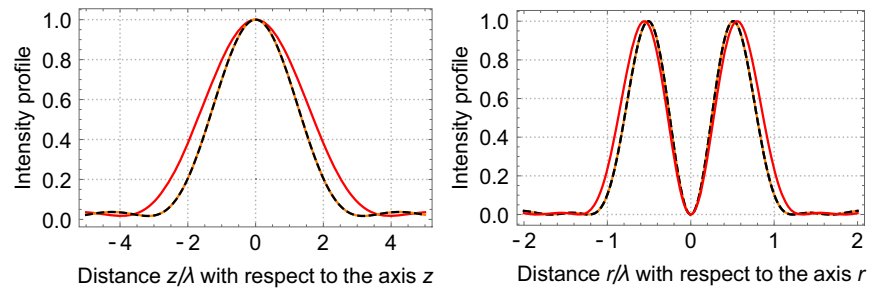
Fig. 1 Normalized intensity profiles of several microscope objectives. On the left is the profile along z and on the right is a long r. The black line coincides with the diffraction pattern of a perfect spherical wavefront at the exit pupil computed with the classical formulation of Richards–Wolf.[4,5] The dashed orange and red lines correspond to the results of the microscope objective in Tables 1 and 2, respectively.
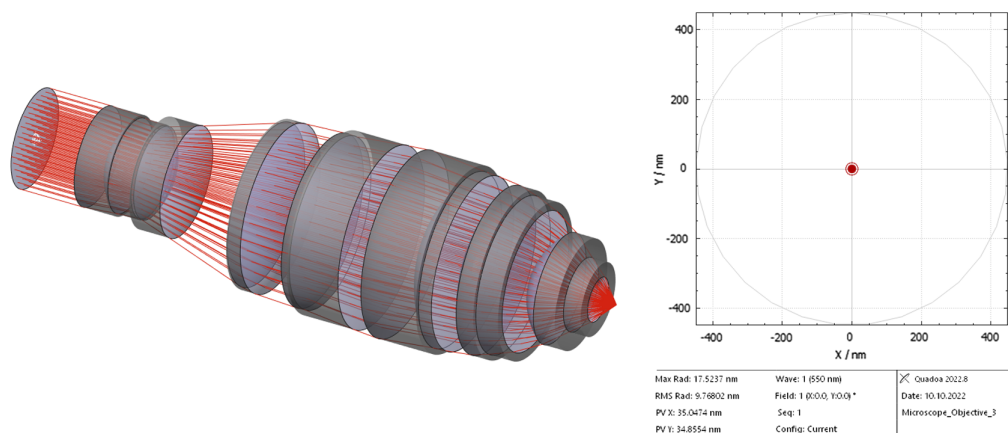
Fig. 2 Microscope objective of Table 1. At left is the ray tracing and at right is the spot diagram.

Table 1 Specifications of the microscope of Fig. 2.

Radius (mm)	Thickness (mm)	Index	Aperture (mm)
inf	5.0	Air	4.0
20.5533	1.5	1.73249	4.0
5.09748	3.0	1.69404	3.76865
12.265	2.0	Air	3.65133
−6.21604	2.0	1.45747	3.67833
−16.8403	6.0	Air	4.44219
100.259	3.0	1.45747	6.49604
−15.4398	1.0	Air	6.72081
24.3013	4.0	1.45747	6.88895
−11.3619	2.5	1.81235	6.84647
−57.9376	0.1	Air	7.27017
19.4423	3.5	1.54999	7.4213
10.3049	4.0	1.45747	6.95852
−87.3925	0.0	Air	6.90845
v13.9012	3.5	1.73249	6.69251
−60.78	1.5	1.4882	6.27531
213.532	0.0	Air	5.59196
5.63103	3.5	1.75856	4.42499
9.21752	1.5	1.81235	2.93
3.91087	2.0	Air	1.77405

described by the Fraunhofer approximation. The design parameters of this microscope are presented in Table 1.

The next example is another microscope objective that has a nearly diffraction-limited spot diagram, also with an NA = 0.749. The ray tracing and the spot diagram of this example can be seen in Fig. 3. The specifications are in Table 2. The profile of the diffraction pattern has been added in Fig. 1, under the red lines. The performance of this microscope objective is below the
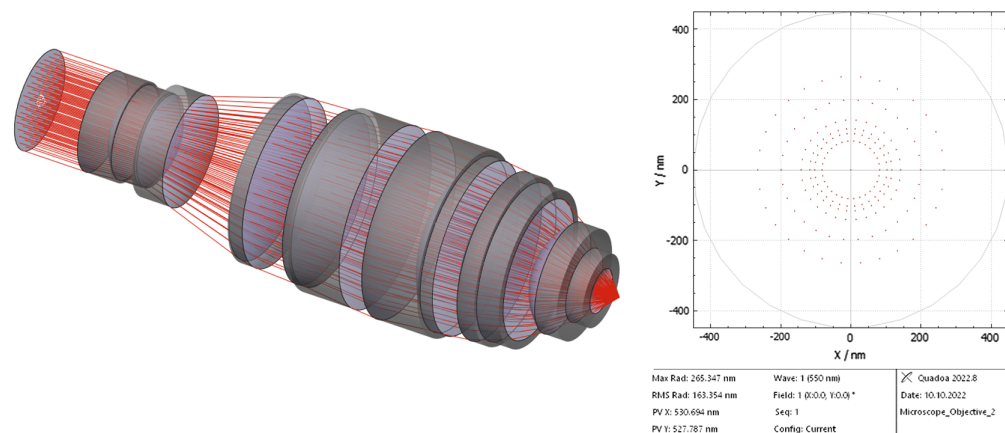
Fig. 3 Microscope objective of Table 2. At left is the ray tracing and at right is the spot diagram.

Table 2 Specifications of the microscope of Fig. 3.

Radius (mm)	Thickness (mm)	Index	Aperture (mm)
inf	5.0	Air	4.0
21.2506	1.5	1.73249	4.0
5.13186	3.0	1.69404	3.77608
12.4164	2.0	Air	3.66356
−6.3095	2.0	1.45747	3.69292
−17.5105	6.0	Air	4.45573
96.969	3.0	1.45747	6.52555
−15.3181	1.0	Air	6.74518
24.0349	4.0	1.45747	6.90953
−11.3122	2.5	1.81235	6.86821
−57.7372	0.1	Air	7.29367
19.5144	3.5	1.54999	7.44342
10.5222	4.0	1.45747	6.98391
−88.3667	0.0	Air	6.92892
13.9311	3.5	1.73249	6.70706
−63.2024	1.5	1.4882	6.28521
199.153	0.0	Air	5.60167
5.63528	3.5	1.75856	4.43241
9.47958	1.5	1.81235	2.94718
3.94334	2.0	Air	1.78282

other examples, as expected. It is diffraction-limited, but its geometrical spot size is bigger than the first example. Its full width at half maximum for the radial dimension is 1.2λ and 0.701λ for the on-axis component for the positive refraction index. The Zernike coefficients for this example are $z_1 = -3.1164 \times 10^{-04}$, $z_4 = 3.2019 \times 10^{-04}$, $z_{11} = -1.1323 \times 10^{-05}$, and $z_{22} = -4.6723 \times 10^{-05}$.

The results presented for the two microscopes are very illustrative since they show how two different systems with similar NA and can be considered diffraction-limited by geometrical optics and scalar diffraction theory they present different performances with a vectorial treatment.

There are other methods to compute diffraction patterns in similar circumstances. They are mostly based on the paradigm presented in Refs. 15, 24, and 25. Reference 15 considers no aberrations, which he explicitly mentions in the mentioned paper before Eq. (5). Thus, its method is not considered directly the same problem that we consider in our manuscript. The difference between our method and Refs. 24 and 25. The derivations presented in Refs. 24 and 25 are too cumbersome in comparison with our method. Our method is straightforward. We only use eight equations, instead of 52 and 38 presented in Refs. 24 and 25, respectively. Our method does not need additional so-called optical coordinates, like in Refs. 24 and 25. Since our method comes from an expression that works for freeform wavefronts, Eq. (2). We do not need to use concepts like surfaces of revolution as our initial premise as can be seen in Eqs. (6) and (7) in Ref. 24 or Eq. (5) in Ref. 25.

References 24 and 25 are just limited to some Seidel coefficients. Our method works directly with an explicit wavefront function w. The computation of the method in Ref. 24 implies several approximations that we do not consider. To mention a few Eq. (27), the expression after Eq. (28)

(not numbered in the paper), the expression after Eq. (35) (not numbered in the paper), and Eqs. (51) and (52). Reference 25 considers small aberrations, something we do not consider. It is explicitly mentioned before Eq. (20) in Ref. 25. Reference 25 considers several approximations that also we do not consider, such as their Eqs. (20), (21), (22), and (43). Also, it is not clear and the author does not mention in Refs. 24 and 25, that the propagation vector is normal to the wavefront, something that is a crucial step in our manuscript.

The approach outlined in this study diverges from the numerical strategy outlined in Ref. 29. In contrast, the method proposed by Wang in Ref. 29 relies on numerical approximations, such as the homeomorphic Fourier transform. The derivation of the closed-form equation Eq. (8) in our method is entirely analytical, devoid of any reliance on numerical approximations or iterative processes. In our manuscript, we can reduce our expressions to a single integral if and only if the wavefront is a surface of revolution and the polarization angle θ is constant.

It is important to remark that this analysis is not restricted to microscope objectives, but it can be applied in the radially symmetric optical system in general. Equation (8) can be used directly with the coefficients extracted from available tools. The natural step to follow in this research is to consider miss alignment and off-axial fields. This generalization considerably increases the complexity of the system and its non-linearity since the direction of the polarization in every point of the wavefront $w(x, y)$ changes due to polarization aberrations.[30] That problem is complex enough to be treated apart in a specific manuscript.

4 Conclusions

In this manuscript, we have derived an integral to compute the diffraction pattern of on-axis beams for radially symmetric systems, with radial polarization, Eq. (8). To validate Eq. (8), we tested it with a perfect spherical wavefront. The results are equal to the ones presented in the classical formulation of Richards–Wolf.[4,5] Then, we compare two different microscope objectives and the results were as predicted by the theory presented in this work.

Disclosures

The author declares no conflicts of interest.

Code and Data Availability

Data underlying the results presented in this paper are not publicly available at this time but may be obtained from the author upon reasonable request.

Funding

References

1. M. Born and E. Wolf, *Principles of Optics: Electromagnetic Theory of Propagation, Interference and Diffraction of Light*, Elsevier (2013).
2. J. Braat and P. Török, *Imaging Optics*, Cambridge University Press (2019).
3. C. S. Williams and O. A. Becklund, *Introduction to the Optical Transfer Function*, Vol. **112**, SPIE Press, Bellingham, Washington (2002).
4. E. Wolf, "Electromagnetic diffraction in optical systems-I. An integral representation of the image field," *Proc. R. Soc. Lond. Ser. A Math. Phys. Sci.* **253**(1274), 349–357 (1959).
5. B. Richards and E. Wolf, "Electromagnetic diffraction in optical systems, II. Structure of the image field in an aplanatic system," *Proc. R. Soc. Lond. Ser. A Math. Phys. Sci.* **253**(1274), 358–379 (1959).
6. G. Thériault, Y. De Koninck, and N. McCarthy, "Extended depth of field microscopy for rapid volumetric two-photon imaging," *Opt. Express* **21**(8), 10095–10104 (2013).
7. F. O. Fahrbach et al., "Light-sheet microscopy in thick media using scanned Bessel beams and two-photon fluorescence excitation," *Opt. Express* **21**(11), 13824–13839 (2013).
8. J. Liu et al., "Rigorous theory on elliptical mirror focusing for point scanning microscopy," *Opt. Express* **20**, 6175–6184 (2012).
9. J. Liu, Ed., *Elliptical Mirrors*, pp. 2053–2563, IOP Publishing (2018).

10. Q. Zhan, "Trapping metallic Rayleigh particles with radial polarization," *Opt. Express* **12**(15), 3377–3382 (2004).
11. C. Varin, M. Piché, and M. A. Porras, "Acceleration of electrons from rest to gev energies by ultrashort transverse magnetic laser pulses in free space," *Phys. Rev. E* **71**(2), 026603 (2005).
12. D. Sugic et al., "Knotted polarizations and spin in three-dimensional polychromatic waves," *Phys. Rev. Res.* **2**(4), 042045 (2020).
13. M. F. Ferrer-Garcia et al., "Polychromatic electric field knots," *Phys. Rev. Res.* **3**(3), 033226 (2021).
14. K. Jahn and N. Bokor, "Solving the inverse problem of high numerical aperture focusing using vector Slepian harmonics and vector Slepian multipole fields," *Opt. Commun.* **288**, 13–16 (2013).
15. R. Kant, "An analytical solution of vector diffraction for focusing optical systems," *J. Mod. Opt.* **40**(2), 337–347 (1993).
16. A. April, P. Bilodeau, and M. Piché, "Focusing a TM 01 beam with a slightly tilted parabolic mirror," *Opt. Express* **19**(10), 9201–9212 (2011).
17. S. Quabis et al., "The focus of light–theoretical calculation and experimental tomographic reconstruction," *Appl. Phys. B* **72**(1), 109–113 (2001).
18. H. Dehez, A. April, and M. Piché, "Needles of longitudinally polarized light: guidelines for minimum spot size and tunable axial extent," *Opt. Express* **20**(14), 14891–14905 (2012).
19. A. April and M. Piché, "4Π Focusing of TM_{01} beams under nonparaxial conditions," *Opt. Express* **18**(21), 22128 (2010).
20. R. G. González-Acuña, "Stigmatic singlet with a user-defined apodization pupil function," *JOSA A* **39**(2), 213–218 (2022).
21. R. G. González-Acuña, J. Borne, and S. Thibault, "On the diffraction of a high-NA aplanatic and stigmatic singlet," *JOSA A* **38**(9), 1332–1338 (2021).
22. R. G. González-Acuña and S. Thibault, "Exact vectorial model for nonparaxial focusing of freeform wavefronts," *Opt. Express* **30**(13), 23656–23663 (2022).
23. R. G. González-Acuña and S. Thibault, "General diffraction integral for converging freeform vectorial fields," *Phys. Script.* **98**(11), 115503 (2023).
24. R. Kant, "An analytical solution of vector diffraction for focusing optical systems with Seidel aberrations: I. spherical aberration, curvature of field, and distortion," *J. Mod. Opt.* **40**(11), 2293–2310 (1993).
25. R. Kant, "An analytical method of vector diffraction for focusing optical systems with Seidel aberrations II: astigmatism and coma," *J. Mod. Opt.* **42**(2), 299–320 (1995).
26. R. Kingslake and R. B. Johnson, *Lens Design Fundamentals*, Academic Press (2009).
27. F. Bowman, *Introduction to Bessel Functions*, Courier Corporation (2012).
28. *Quadoa Optical CAD Software Manual v.*, Quadoa Optical Systems (2022).
29. Z. Wang et al., "Generalized debye integral," *Opt. Express* **28**(17), 24459–24470 (2020).
30. R. A. Chipman, W.-S. T. Lam, and G. Young, *Polarized Light and Optical Systems*, CRC Press (2018).

Rafael G. González-Acuña studied industrial physics engineering at the Tecnológico de Monterrey and received his master's degree in optomechatronics at the Optics Research Center, A.C. He studied PhD at the Tecnológico de Monterrey. He has 37 papers in indexed journals. He has been awarded the 2019 Optical Design and Engineering Scholarship by SPIE and is the co-author of two IOP books: *Analytical Lens Design and Stigmatic Optics*.

Simon Thibault received his BSc degree in physics engineering in 1994 and his MS degree in physics in 1995 from Laval University (Québec, Canada). He completed his PhD in optical system design in 1998 at the same university and after five years as head of the optical design department at the National Optical Institute (INO) in Québec. He joined ImmerVision (Montréal, Canada) in 2005 as principal optical designer and director – Optical Division. He has authored and co-authored 12 patents and over 100 technical communications and papers for renowned optics conferences and journals.